

IET Renewable Power Generation

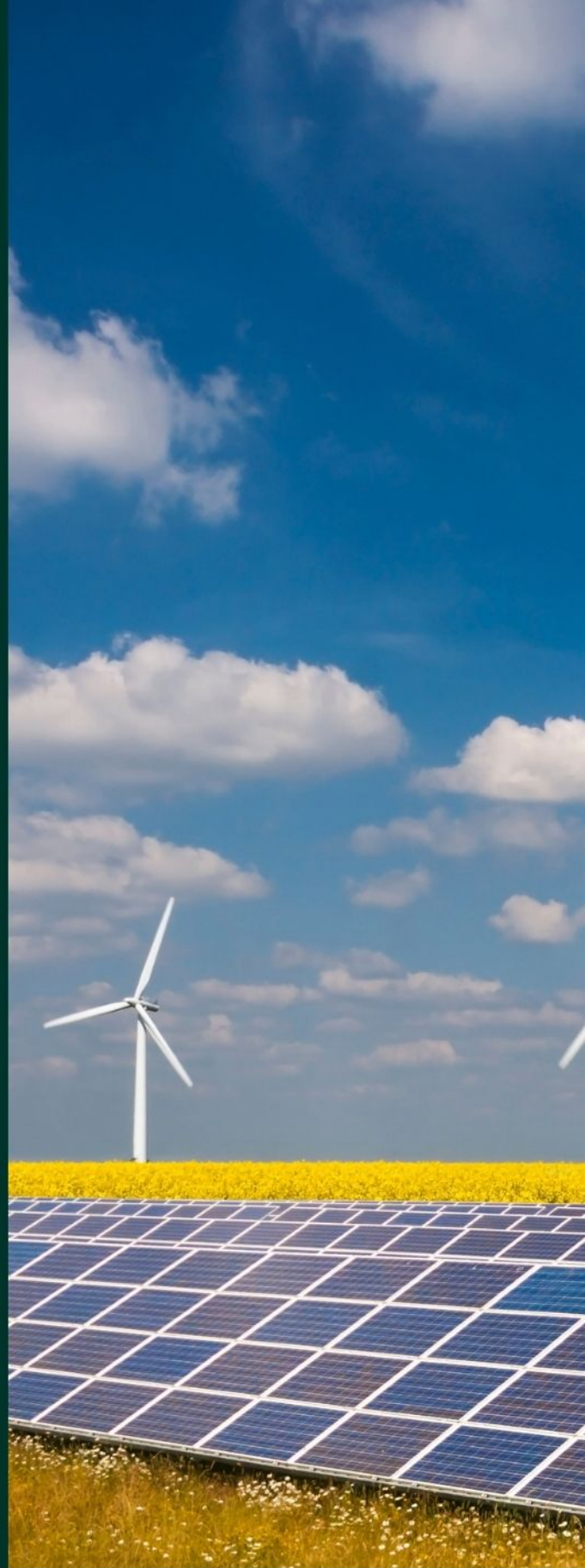
Special Issue Call for Papers

**Be Seen. Be Cited.
Submit your work to a new
IET special issue**

Connect with researchers and
experts in your field and
share knowledge.

Be part of the latest research
trends, faster.

[Read more](#)



The Institution of
Engineering and Technology

Importance of drivetrain optimisation to maximise electrical power from wave energy converters

Nataliia Y. Sergiienko  | Leandro Souza Pinheiro da Silva | Boyin Ding | Benjamin S. Cazzolato

School of Mechanical Engineering, University of Adelaide, Adelaide, Australia

Correspondence

Nataliia Y. Sergiienko, School of Mechanical Engineering, University of Adelaide, SA, 5005, Australia.
Email: nataliia.sergiienko@adelaide.edu.au

Abstract

This article demonstrates the benefits of optimising the drivetrain to improve the level and quality of electrical power output from a wave energy converter. The study considers a spherical buoy connected to a permanent magnet synchronous generator through a mechanical drive. The wave energy converter is equipped with a model predictive control system that maximises electrical power from the generator. Three different scenarios are compared: (i) when the drivetrain is not optimised, (ii) when only the gear ratio is optimised, (iii) and when both gear ratio and flywheel inertia are optimised. The performance of all three configurations is compared in terms of their effect on the generator operating range, the natural frequency of the system, the amount of generated electrical power, and control forces. The results demonstrate that the drivetrain optimisation leads to a significant increase in the electrical power output while shifting the generator's operating range to areas with the highest efficiency. Moreover, drivetrain designs that utilise a flywheel reduce the power take-off loads and facilitate smoother power production.

1 | INTRODUCTION

Wave energy converters (WECs) are designed to absorb energy from ocean waves and convert it into electricity. Any WEC is a complex system that consists of a structure that interacts with waves, a power take-off (PTO) system that converts mechanical or fluid power into electricity, a controller that determines the amount of load applied to the structure from the PTO unit, and power electronics that connects the system to the grid [1]. When designing one of these subsystems, it is necessary to consider the performance and requirements of other components to achieve the optimal design solution from the techno-economic point of view [2].

To date, the wave energy community has mainly focused on improving the hydrodynamic efficiency of the structure (shape or geometry optimisation [3]), developing active control systems that maximise mechanical power [4, 5], and coupling geometry optimisation and control strategy selection [6]. In this regard, the dynamics of the PTO machinery and the electrical part of

the power conversion chain are usually omitted or assumed to be perfect. However, power losses that occur during the power transmission and power generation stages significantly affect the real power production of the WEC [1]. Therefore, focusing only on hydrodynamic performance and mechanical power may mislead design solutions [7], lead to ineffective control algorithms [8] and unrealistic expectations from a device [9].

To fill this gap, a number of studies have developed and validated wave-to-wire models experimentally for WECs with different PTO systems [10]. Thus, it has been shown that relatively simple electro-mechanical models of electrical generators and power converters can capture most power losses [11] and are suitable to be used for the WEC design optimisation [12, 13]. In direct mechanical drive power take-off systems, the WEC is connected to a rotary generator through a drivetrain that converts the linear motion of a buoy into the angular rotation of the generator shaft [14]. Existing electric generators are designed to operate with the maximum efficiency at full load conditions and experience substantial losses during partial load operation [15].

This is an open access article under the terms of the [Creative Commons Attribution](https://creativecommons.org/licenses/by/4.0/) License, which permits use, distribution and reproduction in any medium, provided the original work is properly cited.

© 2021 The Authors. *IET Renewable Power Generation* published by John Wiley & Sons Ltd on behalf of The Institution of Engineering and Technology

Therefore, the drivetrain and control system should be designed to ensure the most efficient transmission of motion and forces from the buoy to the generator.

Few studies available in the public domain have incorporated the drivetrain dynamics (or associated losses) in their wave-to-wire models. Eriksson [16] and Zhou [17] have used an existing design of the PTO machinery with two flywheels to develop a reactive control system for the CorPower device. However, the generator model was not included in the dynamics of the WEC, and its effect on power generation was only represented by the power conversion efficiency coefficient. Similarly, Sjolte et al. [18] have investigated an already designed PTO system including the drivetrain, the generator and the power converter, quantified losses and corresponding power efficiency using experimental campaign and used these results when calculating electrical power generated by a WEC. Also, a number of studies have considered a flywheel energy storage system [19, 20] to smooth the power fluctuations of a WEC and improve its power output. However, the main focus has been given to the choice of the generator configuration while using pre-selected flywheel inertia. A variable inertia hydraulic flywheel has been used in [21] to adjust the inertia of the floating buoy to the incoming wave in real time. The results demonstrate that the proposed system can significantly improve the power production of a WEC, but its benefits over the fixed inertia flywheel require further investigation. Integrated optimisation of the WEC geometry, gearbox, and control parameters has been performed by Sirigu et al. [2] based on several objective functions including power generation and capital expenditures. However, the generator dynamics has not been included in the WEC model, and its performance has been replaced by an efficiency coefficient independent of the drivetrain configuration.

Building upon existing literature, the present work aims to take an additional step forward towards the optimal design of a wave energy converter with a particular focus on the drivetrain design. The main contribution of this paper that distinguish this work from above mentioned studies is twofold: (i) to demonstrate the importance of including a full generator model with load-dependent efficiency in the system optimisation; and (ii) to demonstrate how the drivetrain design affects the operating range of the generator and the hydrodynamic performance of the entire system. As a result, different configurations of the drivetrain are optimised for the given buoy, generator, and control system to improve the electrical power generated by the WEC. The case study used in the paper is a spherical floating buoy connected to a permanent magnet synchronous generator, together with a model predictive control to maximise electrical power from the generator.

2 | WAVE-TO-WIRE MODEL OF A WAVE ENERGY CONVERTER

A generic floating half-submerged sphere that absorbs power from one degree-of-freedom, heave, is chosen as a case study (see Figure 1). The buoy is directly connected to the mechanical

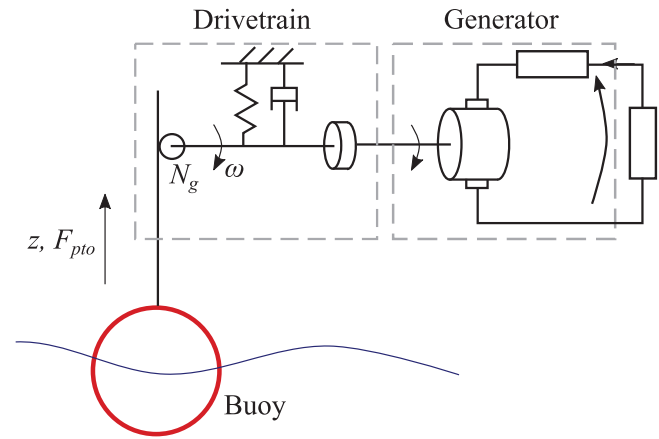


FIGURE 1 Schematic of the wave energy converter (adapted from [13])

TABLE 1 Parameters of the WEC and PTO unit

Parameter	Value
WEC	
Buoy radius, a	5 m
Water depth, b	50 m
Mass, m	1.99×10^6 kg
Initial drivetrain	
Gear ratio, N_g	38.5 rad/m
Generator	
Generator	PMSM
Rated power	83.7 kW
Maximum torque	3700 Nm
Nominal speed	400 rpm
Maximum speed	1800 rpm
Number of poles, N_p	28
Stator resistance, R_s	0.038 Ω
Stator inductance, L_s	1.4 mH
Generator inertia, I_g	1.31 kg m ²
Permanent magnet flux, λ_{PM}	0.257 Wb

drive PTO system that consists of a drivetrain and a rotary generator.

The drivetrain is presented as a system with inertia (flywheel), a torsional spring, and a damper representing mechanical losses. A surface-mounted permanent magnet synchronous machine (PMSM) designed for the Fred Olsen BOLT Lifesaver project is used in this study due to its publicly available detailed specifications [15, 22]. As this PMSM can operate in both generator and motor modes, it is suitable for the reactive control of the WEC [15]. Parameters of the entire system are specified in Table 1.

2.1 | Hydrodynamic model of the WEC

The vertical motion of the buoy under the wave and power take-off loads can be described by the following equation:

$$m\ddot{z}(t) = F_{\text{exc}}(t) + F_{\text{rad}}(t) + F_{\text{hs}}(t) + F_{\text{pto}}(t), \quad (1)$$

where

F_{exc} is the wave excitation force;

F_{rad} is the wave radiation force modelled as:

$$F_{\text{rad}} = -A_{\infty}\ddot{z} - \int_{-\infty}^t K_{\text{rad}}(t-\tau)\dot{z}(\tau)d\tau \equiv -A_{\infty}\ddot{z} - F_r, \quad (2)$$

where A_{∞} is the infinite frequency added mass coefficient, and $K_{\text{rad}}(t)$ is a retardation function, and F_r is replaced by a state-space model using the Marine System Simulator toolbox developed by Perez and Fossen in [23]:

$$\begin{aligned} \dot{\mathbf{p}}_r &= \mathbf{A}_r\mathbf{p}_r + \mathbf{B}_r\dot{z}, \\ F_r &= \mathbf{C}_r\mathbf{p}_r. \end{aligned} \quad (3)$$

Here, $\mathbf{p}_r \in R^{4 \times 1}$ is an auxiliary vector without any physical meaning (for details see [24]), \mathbf{A}_r , \mathbf{B}_r , and \mathbf{C}_r are the state space matrices. The frequency-dependent coefficients of the excitation and radiation forces are obtained using WAMIT [25]; F_{hs} is the linearised net restoring force:

$$F_{\text{hs}}(t) = -K_{\text{hs}}z(t) = -\rho g \pi a^2 z(t), \quad (4)$$

where K_{hs} is the hydrostatic stiffness, ρ is the water density, and g is the acceleration of gravity;

F_{pto} is the force exerted on the buoy from the PTO unit.

2.2 | Drivetrain dynamics

The vertical velocity of the buoy (\dot{z}) and PTO force (F_{pto}) are converted to the rotational (mechanical) speed of the shaft (ω_m) and mechanical torque (T_m) using the gear ratio (N_g) as:

$$\omega_m = \dot{z}N_g, \quad T_m = \frac{F_{\text{pto}}}{N_g}. \quad (5)$$

According to [26], the drivetrain dynamics can be modelled as a linear mass-spring-damper system:

$$I_d\dot{\omega}_m = T_c - T_m - B_d\omega_m - K_d\theta_m, \quad (6)$$

where θ_m is the angular displacement of the shaft with respect to the reference/ground, T_c is the electromagnetic torque from the generator, I_d is the drivetrain inertia (including the genera-

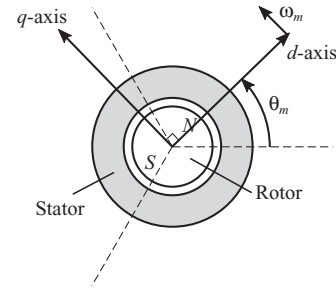


FIGURE 2 dq reference frame of the PMSM [27]

tor inertia I_g), B_d is the drivetrain and generator shaft viscous friction, and K_d is the drivetrain stiffness coefficient.

2.3 | Rotary generator model

The electro-mechanical equations of the PMSM are adapted from [27] and presented in the rotating dq reference frame (d -axis is always aligned with the rotor magnetic axis, q -axis is 90° ahead in the direction of rotation), as shown in Figure 2. The voltage equations for the stator are [27]:

$$V_{sd} = R_s i_{sd} + L_s \frac{d}{dt} i_{sd} - \omega_e L_s i_{sq}, \quad (7)$$

$$V_{sq} = R_s i_{sq} + L_s \frac{d}{dt} i_{sq} + \omega_e (L_s i_{sd} + \lambda_{\text{PM}}), \quad (8)$$

where i_{sd} and i_{sq} are the currents in the dq axes, R_s is the stator winding resistance, L_s is the stator inductance, ω_e is the rotor electric frequency in rad/s, and λ_{PM} is the rotor permanent magnet flux.

The speed ω_e is related to the actual mechanical rotor speed ω_m as:

$$\omega_e = \frac{N_p}{2} \omega_m, \quad (9)$$

where N_p is the number of poles.

The electromagnetic torque generated by the PMSM is:

$$T_c = \frac{3N_p}{4} i_{sq} \lambda_{\text{PM}} = k_T i_{sq}, \quad (10)$$

where $k_T = 3/4 N_p \lambda_{\text{PM}}$ is the torque constant.

When the generator operates in the normal speed range (below rated), the d -axis current is kept as 0 ($i_{sd} = 0$). When the rated speed is exceeded, the field weakening ($i_{sd} < 0$) technique is used to keep the back-EMF from exceeding the rated voltage of the motor. According to [28], the field weakening speed of this PMSM is 561 rpm (58 rad/s). For simplicity, it is assumed that the generator velocity will not exceed this value, so d -axis current is set to 0 A, and only Equation (8) will be used further.

2.4 | Combined wave-to-wire model

Combining Equations (1)–(10), it is possible to derive the wave-to-wire model of the system shown in Figure 1 in a state-space form:

$$\dot{\mathbf{x}}_c = \mathbf{A}_c \mathbf{x}_c + \mathbf{B}_c u_c + \mathbf{F}_c v_c, \quad (11)$$

$$\mathbf{y}_c = \mathbf{C}_c \mathbf{x}_c, \quad (12)$$

where the state vector \mathbf{x}_c , the output vector \mathbf{y}_c , the control variable u_c and the external input v_c are defined as:

$$\mathbf{x}_c = \begin{bmatrix} \tilde{\chi} \\ \dot{\tilde{\chi}} \\ i_{sq} \\ \mathbf{p}_r \end{bmatrix}, \quad \mathbf{y}_c = \begin{bmatrix} \tilde{\chi} \\ i_{sq} \end{bmatrix}, \quad u_c = V_{sq}, \quad v_c = \frac{F_{exc}}{I_c}, \quad (13)$$

$I_c = m + A_\infty + I_d N_g^2$ is used to denote the effective inertia of the system, and the state space matrices are:

$$\mathbf{A}_c = \begin{bmatrix} 0 & 1 & \mathbf{0}_{1,4} & 0 \\ \frac{-K_{hs} - K_d N_g^2}{I_c} & \frac{-B_d N_g^2}{I_c} & \frac{k_T N_g}{I_c} & \frac{-\mathbf{C}_r}{I_c} \\ 0 & \frac{-2 k_T N_g}{3 L_s} & \frac{-R_s}{L_s} & \mathbf{0}_{1,4} \\ \mathbf{0}_{4,1} & \mathbf{B}_r & \mathbf{0}_{4,1} & \mathbf{A}_r \end{bmatrix}, \quad (14)$$

$$\mathbf{B}_c = \begin{bmatrix} 0 \\ 0 \\ 0 \\ 1/L_s \end{bmatrix}, \quad \mathbf{F}_c = \begin{bmatrix} 0 \\ 1 \\ 0 \\ 0 \end{bmatrix}, \quad \mathbf{C}_c = \begin{bmatrix} 1 & 0 & \mathbf{0}_{1,4} & 0 \\ 0 & 0 & \mathbf{0}_{1,4} & 1 \end{bmatrix}. \quad (15)$$

2.5 | Power output

The average mechanical power absorbed by the WEC over a period of time T is:

$$\bar{P}_{mech} = -\frac{1}{T} \int_0^T F_{pto}(t) \dot{\tilde{\chi}}(t) dt = -\frac{1}{T} \int_0^T T_m(t) \omega_m(t) dt. \quad (16)$$

The average electrical power generated by the generator is equal to [11]:

$$\bar{P}_{elec} = -\frac{3}{2} \frac{1}{T} \int_0^T i_{sq}(t) V_{sq}(t) dt. \quad (17)$$

2.6 | Control system

The WEC is equipped with a model predictive control (MPC) system that maximises electrical (not mechanical) power out-

put. Due to the cumbersome equations that define the MPC, the algorithm, including the discretisation of the continuous-time system, system prediction and formulation of the objective function, are outlined in the Appendix. In general, at each time step, the controller uses predicted values of the excitation force F_{exc} as well as the dynamic wave-to-wire model of the WEC, Equations (11)–(12), and attempts to find values of the generator voltage V_{sq} such that the average electrical power generated by the WEC over the prediction horizon T_h is maximised. For this study, the prediction process of the wave excitation force is assumed to be perfect. The controller optimisation problem is formulated as a quadratic cost function with linear constraints (the maximum DC-bus current is limited by 481 A).

3 | DRIVETRAIN OPTIMISATION

The drivetrain optimisation process has been performed using `fbWECCntrl` MATLAB toolbox developed by Sandia National Laboratories, US [12]. This toolbox uses an in-built MATLAB solver `fmincon` to find optimal PTO variables, in particular, drivetrain configuration and control parameters, that maximise electrical power in a given sea state assuming a causal impedance matching control approach [29]. The optimisation is done in the frequency domain assuming linear dynamics of the WEC, the drivetrain and the generator, and does not take into account any motion or force constraints. The default interior-point optimisation algorithm is used with the maximum number of function evaluations and the maximum number of iterations set to 10^6 .

According to Figure 1, parameters of the drivetrain that can be optimised include the gear ratio N_g , the stiffness coefficient K_d , and the flywheel inertia I_d . The main focus in this study is given to N_g and I_d variables only. The optimal value of the stiffness K_d for this case study always turned out to be negative due to the presence of hydrostatic stiffness. This value is considered impractical even though some engineering solutions exist to achieve negative stiffness using the magnetic system. So $K_d = 0$ is kept fixed and is not considered as the optimisation variable.

This study does not intend to optimise the drivetrain parameters for a specific location, but rather to demonstrate what effects the optimal design has on the generator operating region, power quality, required PTO forces, and power conversion efficiency. Moreover, optimisation results obtained using `fbWECCntrl` MATLAB toolbox are insensitive to the wave height due to the linear dynamics assumption. Hence, the value of the generated power is proportional to the square of the wave height leading to the same optimised parameters regardless of the wave height value. As a result, the analysis is presented for a range of sea states with different peak wave periods and a fixed significant wave height.

3.1 | Initial (not optimised) drivetrain

The PMSM generator specified in Table 1 was designed for the Fred Olsen BOLT Lifesaver project to be used with a

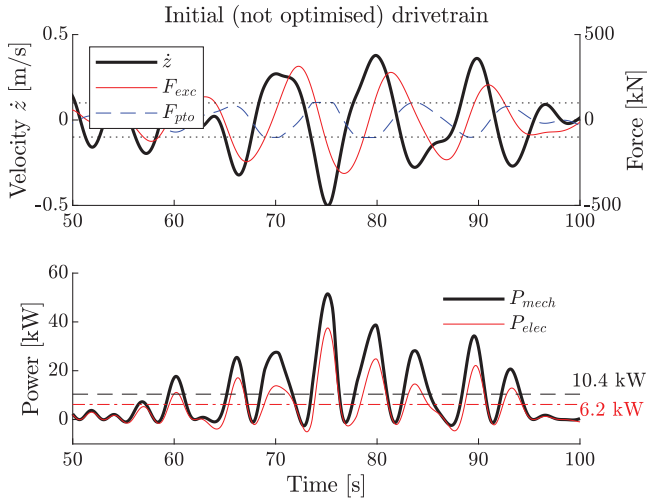


FIGURE 3 Performance of the WEC (motion, forces, and power output) in the irregular wave of $H_s = 1$ m and $T_p = 10$ s with the initial drivetrain design. The WEC is actively controller by the MPC

gearbox $N_g = 38.5$ rad/m. As the generator current is limited by 481 A, the maximum PTO force that can be exerted on the buoy with this gear ratio is 100 kN ($F_{pto}^{max} = N_g T_m^{max} = N_g k_{T_{sq}}^{max} = 38.5$ rad/m \cdot 5.397 Nm/A \cdot 481 A = 100 kN). Figure 3 demonstrates the performance of the WEC with the initial drivetrain configuration in the irregular sea state of $H_s = 1$ m, and $T_p = 10$ s defined by a Bretschneider spectrum [30]. The WEC is actively controlled by the model-predictive controller.

As the initial drivetrain is not optimised for the WEC/generator combination, and MPC is designed to maximise electrical (not mechanical) power, the WEC velocity is not in phase with the excitation force leading to poor hydrodynamic efficiency. The control force reaches its maximum value of 100 kN at almost every cycle. This situation is undesirable from the design point of view, which means that the PTO system configuration, in particular, a combination of the PMSM with this drivetrain design, is not suitable for this particular buoy and the control system.

3.2 | Optimisation of the gear ratio

According to Equation (5), the gear ratio determines the operating range of generator torques and speeds, directly affecting the power conversion efficiency of the entire system. Figure 4 shows what should be the value of the gear ratio (with no added flywheel) to maximise electrical power of the WEC/generator system using causal complex-conjugate control across a range of irregular sea states. The drivetrain inertia is assumed to be equal to the generator inertia of $I_d = I_g = 1.31$ kg m^2 . It is clear from Figure 4 that the optimal gear ratio increases with peak wave period. This can be explained by the fact that longer waves require higher control forces and lower buoy velocities. Therefore, to keep the same operating range of the generator torque and speed with mini-

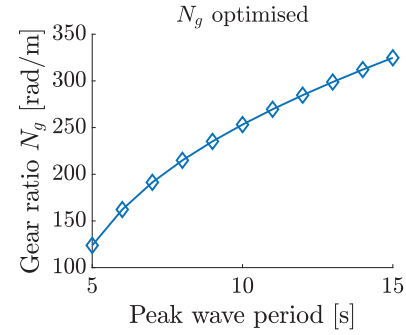


FIGURE 4 Dependence of the optimal gear ratio (no flywheel) on the peak wave period T_p , significant wave height is set to $H_s = 1$ m

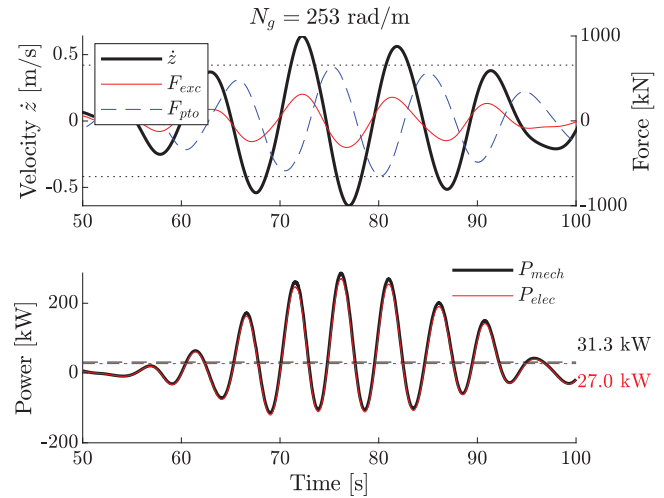


FIGURE 5 Performance of the WEC (motion, forces, and power output) in the irregular wave of $H_s = 1$ m and $T_p = 10$ s with the optimised gear ratio. The WEC is actively controller by the MPC

mal power losses, the gear ratio should be increased as per Equation (5).

The performance of the WEC with an optimised gear ratio of $N_g = 253$ rad/s for the sea state of $H_s = 1$ m and $T_p = 10$ s is demonstrated in Figure 5. As N_g has been increased compared to the initial drivetrain configuration, the maximum allowed control force has increased correspondingly to 657 kN ($F_{pto}^{max} = N_g k_{T_{sq}}^{max} = 253$ rad/m \cdot 5.397 Nm/A \cdot 481 A = 657 kN). Moreover, the average electrical power production has improved significantly (from 6.2 to 27 kW). However, it should be noted that an increase in loads on the PTO system directly affects the design requirements and cost of the mechanical drive. Moreover, some gearbox designs have gear ratio limitations to allow back drive.

3.3 | Optimisation of the gear ratio and drivetrain inertia

The drivetrain inertia can be altered by adding a flywheel to the system. Flywheels act as energy storage and can be used to smooth out the electrical power output. To achieve the best

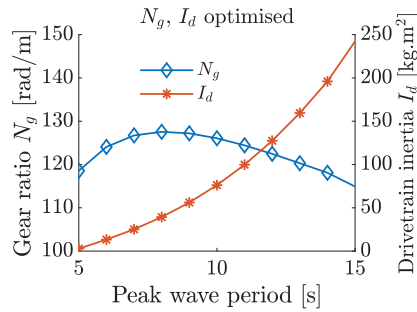


FIGURE 6 Dependence of the optimal gear ratio and flywheel inertia on the peak wave period T_p , significant wave height is set to $H_s = 1$ m

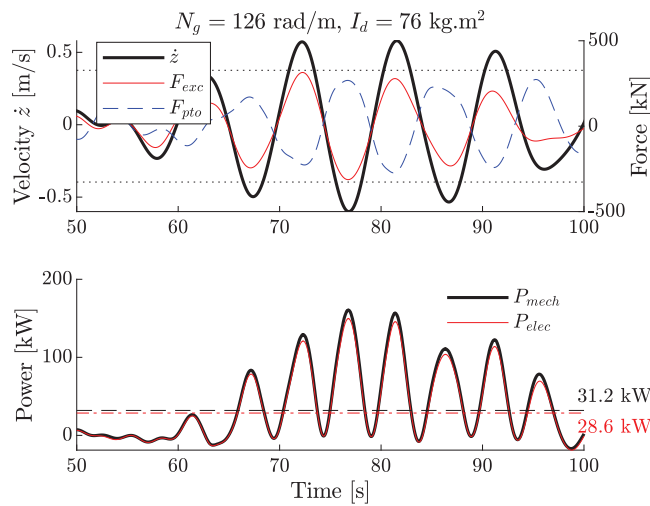


FIGURE 7 Performance of the WEC (motion, forces, and power output) in the irregular wave of $H_s = 1$ m and $T_p = 10$ s with the optimised gear ratio and flywheel inertia. The WEC is actively controlled by the MPC

effect from using flywheels, the drivetrain should be equipped with a clutching mechanism that can engage or disengage the flywheel from the shaft when required. In this study, all the results are presented for the scenario with an engaged flywheel. The simultaneous optimisation of the required gear ratio N_g and drivetrain inertia I_d has been performed using `fbWECCntrl` MATLAB toolbox, and the resultant optimal values are shown in Figure 6 across a range of sea states.

Interestingly, when both parameters are optimised, the required gear ratio is relatively insensitive to the peak wave period and is within a range of 115–130 rad/m. In contrast, the required flywheel inertia increases with a wave period demonstrating that higher energy storage is needed when a WEC operates at sea states characterised by longer wave periods. An example time-series of the WEC performance in a sea state $H_s = 1$ m and $T_p = 10$ s with optimised drivetrain parameters is shown in Figure 7. The limit on the control force has been changed to 327 kN due to the optimised value of $N_g = 126$ rad/m ($F_{pto}^{max} = N_g k_{T_{sq}}^{max} = 126 \text{ rad/m} \cdot 5.397 \text{ Nm/A} \cdot 481 \text{ A} = 327 \text{ kN}$). The level of average power production remains approximately the same as compared to the case when only N_g is optimised (refer to Figure 5). However,

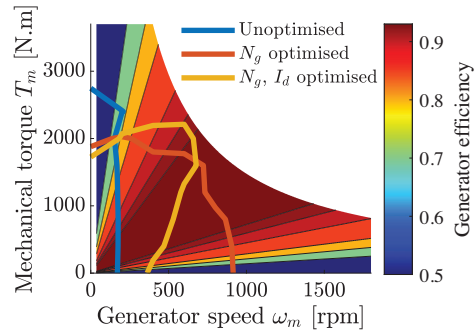


FIGURE 8 Indicative generator operating range in a sea state of $H_s = 1$ m and $T_p = 10$ s for three drivetrain configurations. The motion traces are plotted on top of the generator efficiency map which is calculated as $\eta = \bar{P}_{elec} / \bar{P}_{mech}$ using Equations (6)–(17)

the advantage of adding a flywheel can be clearly seen when comparing instantaneous power output in Figures 5 and 7. In the latter case, the power fluctuations are less, and the electric power remains in the range of positive values.

4 | PERFORMANCE COMPARISON

The drivetrain links the hydrodynamic part of the WEC, a buoy with its hydrodynamic efficiency (wave to mechanical power conversion), to the electrical part of the system, a generator with its efficiency map (mechanical to electrical power conversion). Thus, the generator operating range, in particular, the range of required torques and speeds, is highly dependent on the drivetrain parameters, as demonstrated in Figure 8. The coloured lines indicate the range of speeds and torques experienced by the generator (approximately 90% of the time) in a sea state of $H_s = 1$ m and $T_p = 10$ s for three drivetrain configurations when the WEC is actively controlled by the MPC. This information is shown for 1/4 of the efficiency map only that corresponds to the power generation mode when both speed and torque are positive. When the drivetrain is not optimised, the generator is required to provide high torques at low speeds leading to high power losses. When only N_g is optimised, the generator starts to operate in a wide range of speeds and torques covering areas with higher power conversion efficiency. When both N_g and I_d are optimised, the operating range tends (but not fully aligned) to the area with the highest efficiency.

As Figure 8 is related to the electrical part of the WEC, Figure 9 demonstrates how the drivetrain optimisation affects the hydrodynamic performance of the buoy, in particular its natural period in heave. Thus, for each sea state, an optimal set of N_g and I_d from Figure 6 has been used to calculate the natural frequency as:

$$\omega_n = \sqrt{\frac{K_{hs} + K_d N_g^2}{m + A(\omega_n) + I_d N_g^2}}, \quad (18)$$

where $K_d = 0$ in this study.

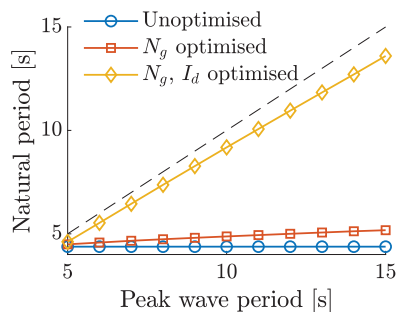


FIGURE 9 The natural period of the WEC with different drivetrain configurations

The natural period of this spherical WEC with the initial drivetrain configuration is 4.4 s, and optimising only N_g (the drivetrain without a flywheel) has minimal effect on the natural period of the system. However, the added inertia from the flywheel allows the natural period to be tuned to the incoming wave. Thus, it can be concluded, that N_g is responsible for optimising the operation of the electrical part, while a combination of N_g and I_d acts to improve the performance of both the hydrodynamic and electrical parts of the WEC. In the latter case, when the buoy is operating close to resonance, there is no need to provide reactive power from the generator, and it will work only in a generator (not motor) mode.

Optimisation results presented in Sections 3.2 and 3.3 have been obtained for a range of sea states using the frequency-domain analysis assuming an approximate complex-conjugate control [29] with no constraints applied to the WEC dynamics. As the drivetrain should be designed for a specific wave climate, it was decided to optimise the drivetrain for one sea state, and test these design configurations in the time domain. Under this scenario, the WEC is actively controlled by the MPC, and the rotor current, and, consequently, the PTO force, is limited. The targeted sea state for drivetrain optimisation, $H_s = 1$ m and $T_p = 10$ s, is chosen arbitrary for this analysis, but is representative of a commonly occurring sea state at many energetic sites. As a result, the performance of the WEC with three different drivetrain configurations (unoptimised, N_g is optimised, and both N_g and I_d are optimised) are compared in Figure 10. The electrical power production of a WEC is shown in Figure 4. The dashed line indicates the maximum mechanical power that can be absorbed by this WEC in each sea state not considering viscous drag losses (refer to the upper bound on the Budal diagram [31]). Both optimised designs demonstrate similar power production levels that are about 5 times higher than that obtained using the initial drivetrain settings.

Breaking down the power conversion chain into two stages, Figure 4 shows the amount of wave power converted into mechanical power, and Figure 4 demonstrates how much of this mechanical power is further converted to electricity using three drivetrain configurations. The WEC with the initial drivetrain design demonstrates the highest hydrodynamic efficiency at sea states with $T_p = 5$ and 6 s, the periods closest to the natural period of this WEC (4.4 s). Nevertheless, the hydro-

dynamic efficiency of this WEC configuration drops significantly at longer wave periods, reaching less than 10% for $T_p > 10$ s. The optimised drivetrain designs improve the wave-to-mechanical power conversion efficiency in the majority of sea states. However, less than half of the maximum possible wave power can be absorbed by the WEC with the optimised drivetrain as the controller is designed to maximise electrical (not mechanical) power. With regard to the conversion of mechanical power into electrical power (refer to Figure 4), the initial drivetrain allowed only 50–70% efficiency, while with optimised designs it is possible to convert up to 93% of mechanical power and the limit is mostly dictated by the generator efficiency map. These results can be related to Figures 8 and 9 demonstrating that the optimised drivetrain improves the hydrodynamic performance and the operating range of the generator at the same time.

Despite similar average power outputs and power conversion efficiencies of the two optimised drivetrains (without and with a flywheel), the quality of the electrical power output is significantly different as demonstrated in Figure 4. The reader is reminded that both configurations have been optimised for a peak wave period of $T_p = 10$ s. The system with a flywheel has a peak-to-average power ratio of approximately 5 at sea states $T_p > 10$ s, while this value for the system without a flywheel is twice higher (≈ 10). However, the chosen flywheel does not benefit the system at lower wave periods due to the lower energy storage capacity requirements. Therefore, the flywheel should be disengaged from the generator shaft at low energy sea states. In addition, the system with a flywheel requires lower control forces from the power take-off system as shown in Figure 4 that may significantly affect the cost of the mechanical drive. Both optimised designs lead to similar motion amplitudes of the WEC as shown in Figure 4, while the system with the initial drivetrain configuration experiences less displacement in heave.

5 | DISCUSSION

This study focuses only on one aspect of the wave energy converter design, namely the drivetrain, while the buoy shape, generator configuration and control system are kept fixed. For the techno-economic optimisation of the entire converter, it is required to consider all of the above-mentioned parameters as optimisation variables to achieve the best design solution for a particular deployment site. Building upon previous work in this domain, it is recommended to extend the existing WEC design optimisation studies to follow the control co-design approach where the buoy parameters (geometry, mass characteristics etc.), drivetrain, generator with its load-dependent efficiency and control system are optimised and designed as an integrated system with the main focus on the electrical power production. Eliminating one or several subsystems from the design optimisation process might lead to sub-optimal solutions and delay competitive wave energy technology development. However, this is out of the scope of the current paper and will be explored in future research.

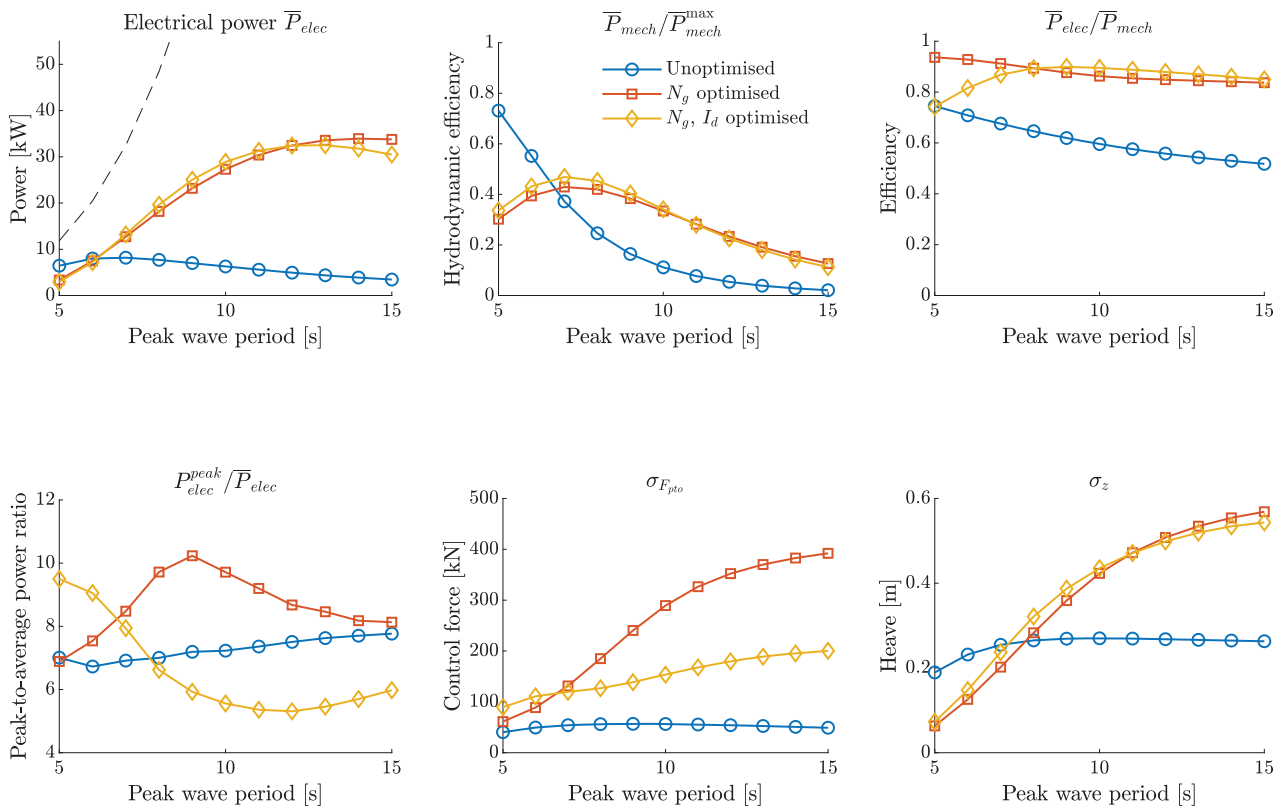


FIGURE 10 Effect of optimised drivetrain configuration on the performance of a wave energy converter: (a) average electrical power output (dashed line corresponds to the maximum amount of energy that can be removed from the sea), (b) wave-to-mechanical power conversion efficiency, (c) mechanical-to-electrical power conversion efficiency, (d) peak-to-average power ratio, (e) standard deviation of the buoy displacement in heave, and (f) standard deviation of the control force. The wave height is set to $H_s = 1$ m. The drivetrain parameters are optimised for a sea state of $H_s = 1$ m, $T_p = 10$ s


6 | CONCLUSION

This paper demonstrates that a drivetrain is an important part of any wave energy converter, so its poor design may lead to significant power losses. The floating buoy and the electrical part have been assumed fixed, while the drivetrain configuration has been optimised for a particular sea state. The main focus has been given to the choice of the gear ratio and flywheel inertia. Also, two cases have been considered: the drivetrain without a flywheel, so only gear ratio is optimised, and the system with a flywheel, when both gear ratio and inertia are optimised. The right choice of these parameters changes the load on the generator making it operate at higher efficiencies. Moreover, the flywheel can be used to tune the WEC natural frequency to the incoming wave exposing fewer requirements on the reactive power flow from the generator. Comparing optimised configurations without and with a flywheel, both of them can lead to the same power production, while the system with a flywheel has half the peak-to-average power ratio and experiences significantly lower loads on the power take-off system.

ACKNOWLEDGMENT

The authors would like to thank Dr. Giorgio Bacelli for his contribution to the development of the idea that led to this research work.

ORCID

Natalia Y. Sergienko  <https://orcid.org/0000-0002-3418-398X>

REFERENCES

1. Penalba, M., Ringwood, J.: A review of wave-to-wire models for wave energy converters. *Energies* 9(7), 506 (2016)
2. Sirigu, S.A., et al.: Techno-economic optimisation for a wave energy converter via genetic algorithm. *J. Mar. Sci. Eng.* 8(7), 482 (2020)
3. Garcia-Teruel, A., Forehand, D.: A review of geometry optimisation of wave energy converters. *Renewable Sustainable Energy Rev.* 139, 110593 (2021)
4. Ringwood, J.V., Bacelli, G., Fusco, F.: Energy-maximizing control of wave-energy converters: The development of control system technology to optimize their operation. *IEEE Control Syst.* 34(5), 30–55 (2014)
5. Faedo, N., Olaya, S., Ringwood, J.V.: Optimal control, MPC and MPC-like algorithms for wave energy systems: an overview. *IFAC J. Syst. Control* 1(Supplement C), 37–56 (2017)
6. Garcia-Rosa, P.B., Ringwood, J.V.: On the sensitivity of optimal wave energy device geometry to the energy maximizing control system. *IEEE Trans. Sustainable Energy* 7(1), 419–426 (2015)
7. Coe, R.G., et al.: Initial conceptual demonstration of control co-design for WEC optimization. *J. Ocean. Eng. Sci. Mar. Energy* 6(4), 441–449 (2020)
8. O'Sullivan, A., Lightbody, G.: Wave to wire power maximisation from a wave energy converter. In: *Proceedings of the 11th European Wave and Tidal Energy Conference*, pp. 1–10. University of Southampton, Southampton (2015)

9. Tedeschi, E., et al.: Effect of control strategies and power take-off efficiency on the power capture from sea waves. *IEEE Trans. Energy Convers.* 26(4), 1088–1098 (2011)
10. Penalba, M., et al.: Validating a wave-to-wire model for a wave energy converter – Part I: the hydraulic transmission system. *Energies* 10(7), 977 (2017)
11. Penalba, M., Cortajarena, J.A., Ringwood, J.V.: Validating a wave-to-wire model for a wave energy converter – Part II: The electrical system. *Energies* 10(7), 1002 (2017)
12. Coe, R.G., Bacelli, G., Forbush, D.: A practical approach to wave energy modeling and control. *Renewable Sustainable Energy Rev.* 142, 110791 (2021)
13. Coe, R., Bacelli, G., Forbush, D.: WEC co-design September 2020 webinar [Presentation]. Sandia National Laboratories, https://youtu.be/iaECUf_H47c (2020). Accessed 30 Sept 2020
14. Têtu, A.: Power take-off systems for WECs. In: Pecher, A., Kofoed, J.P., (eds.) *Handbook of Ocean Wave Energy*, pp. 203–220. Springer, Cham (2017)
15. Sjolte, J., et al.: Exploring the potential for increased production from the wave energy converter lifesaver by reactive control. *Energies* 6(8), 3706–3733 (2013)
16. Eriksson, C.: Model predictive control of CorPower Ocean wave energy converter. Master thesis, KTH, School of Electrical Engineering (2016)
17. Zhou, T.: Damping profile research for CorPower Ocean's wave energy converter. Master thesis, KTH, School of Electrical Engineering (2016)
18. Sjolte, J., et al.: All-electric wave energy power take off system with improved power quality at the grid connection point. In: 2012 EVER International Conference and Exhibition on Ecological Vehicles and Renewable Energies, pp. 1–7. IEEE, Piscataway, NJ (2012)
19. Yoshida, T., et al.: Study of flywheel energy storage system for power leveling of wave power generation system. In: 2012 15th International Conference on Electrical Machines and Systems (ICEMS), pp. 1–5. IEEE, Piscataway, NJ (2012)
20. Helkin, S.A.: Design And optimization of a wave energy harvester utilizing a flywheel energy storage system flywheel energy storage. Master Thesis, University of Central Florida (2011)
21. Binh, P.C., Ahn, K.K.: Performance optimization of dielectric electro active polymers in wave energy converter application. *Int. J. Precis. Eng. Manuf.* 17(9), 1175–1185 (2016)
22. Sjolte, J.: Marine renewable energy conversion: Grid and off-grid modeling, design and operation. Ph.D. Thesis, Norwegian University of Science and Technology (2014)
23. Perez, T., Fossen, T.I.: A Matlab toolbox for parametric identification of radiation-force models of ships and offshore structures. *Model. Identif. Control* 30(1), 1–15 (2009)
24. Sergiienko, N.Y., et al.: Considerations on the optimal control of the three-tether wave energy converter. *Ocean Eng.* 183, 469–477 (2019)
25. Lee, C.H.: WAMIT theory manual. Massachusetts Institute of Technology <https://www.wamit.com/Publications/tmanual.pdf> (1995). Accessed 04 January 2021
26. Bacelli, G., Coe, R.G.: Comments on control of wave energy converters. *IEEE Trans. Control Syst. Technol.* 29(1), 478–481 (2020)
27. Mohan, N.: *Advanced Electric Drives: Analysis, Control, and Modeling using MATLAB/Simulink*. Wiley, New York (2014)
28. Pettersen, M.F., et al.: Effect of non-ideal power take-off on the electric output power of a wave energy converter under suboptimal control. In: Soares, C.G., (eds.) *Developments in Renewable Energies Offshore: Proceedings of the 4th International Conference on Renewable Energies Offshore (RENEW 2020, 12–15 October 2020, Lisbon, Portugal)*, pp. 245–253. CRC Press, Boca Raton, FL (2020)
29. Coe, R.G., et al.: A comparison of control strategies for wave energy converters. *Int. J. Mar. Energy* 20, 45–63 (2017)
30. The Specialist Committee on Waves. Final report and recommendations to the 23rd ITTC. In: *Proceedings of the 23rd International Towing Tank Conference*, vol. II, pp. 505–736. ITTC Association, Zürich (2002)
31. Falnes, J., Hals, J.: 'Heaving buoys, point absorbers and arrays. *Philos. Trans. R. Soc. London, Ser. A* 370(1959), 246–277 (2012)
32. Cretel, J.A., et al.: Maximisation of energy capture by a wave-energy point absorber using model predictive control. *IFAC Proc. Vol.* 44(1), 3714–3721 (2011)
33. Li, G., Belmont, M.R.: Model predictive control of sea wave energy converters – Part I: A convex approach for the case of a single device. *Renewable Energy* 69(2014), 453–463 (2014)

How to cite this article: Sergiienko NY, da Silva LP, Ding B, Cazzolato BS. Importance of drivetrain optimisation to maximise electrical power from wave energy converters. *IET Renew. Power Gener.* 2021;15:3232–3242. <https://doi.org/10.1049/rpg2.12239>

APPENDIX A

A.1 | Discretisation of the continuous-time system

The first-order-hold method, sometimes called triangle approximation, is used to discretise continuous state-space Equation (11) with a sampling interval T_s :

$$\text{for } kT_s \leq t \leq (k+1)T_s,$$

$$\mathbf{u}_d(t) = \mathbf{u}_d(k) + \frac{t - kT_s}{T_s} \Delta \mathbf{u}(k+1),$$

$$\mathbf{v}_c(t) = \mathbf{v}_d(k) + \frac{t - kT_s}{T_s} \Delta \mathbf{v}(k+1),$$

where

$$\Delta \mathbf{u}(k+1) = \mathbf{u}_d(k+1) - \mathbf{u}_d(k),$$

$$\Delta \mathbf{v}(k+1) = \mathbf{v}_d(k+1) - \mathbf{v}_d(k).$$

So the discretised version of Equation (11) can be written as:

$$\begin{aligned} \mathbf{x}_d(k+1) &= \mathbf{\Phi}(T_s) \mathbf{x}_d(k) + \mathbf{\Gamma}_u \mathbf{u}_d(k) + \mathbf{\Gamma}_v \mathbf{v}_d(k) \\ &\quad + \mathbf{\Lambda}_u \Delta \mathbf{u}_d(k+1) + \mathbf{\Lambda}_v \Delta \mathbf{v}_d(k+1), \\ \mathbf{y}_d(k) &= \mathbf{C}_d \mathbf{x}_d, \end{aligned} \quad (\text{A.1})$$

where the discrete-time state transition matrix is $\mathbf{\Phi}(T_s) = e^{\mathbf{A}_c T_s}$, and

$$\mathbf{\Gamma}_u = \mathbf{A}_c^{-1} (\mathbf{\Phi}(T_s) - \mathbf{I}) \mathbf{B}_c \in \mathbb{R}^{n_x \times 1},$$

$$\mathbf{\Gamma}_v = \mathbf{A}_c^{-1} (\mathbf{\Phi}(T_s) - \mathbf{I}) \mathbf{F}_c \in \mathbb{R}^{n_x \times 1},$$

$$\mathbf{\Lambda}_u = \frac{1}{T_s} (\mathbf{\Gamma} - T_s \mathbf{B}_c) \in \mathbb{R}^{n_x \times 1},$$

$$\mathbf{\Lambda}_v = \frac{1}{T_s} (\mathbf{\Gamma} - T_s \mathbf{F}_c) \in \mathbb{R}^{n_x \times 1}.$$

In order to write the objective function for the MPC formulation in terms of the state variables, the state vector \mathbf{x}_d and the output vector \mathbf{y}_d have been augmented as follows:

$$\mathbf{x} = \begin{bmatrix} \mathbf{x}_d \\ \mathbf{u}_d \\ \mathbf{v}_d \end{bmatrix} \in \mathbb{R}^{(n_x+2) \times 1}, \quad \mathbf{y} = \begin{bmatrix} \mathbf{y}_d \\ \mathbf{u}_d \end{bmatrix} \in \mathbb{R}^{(n_y+1) \times 1}.$$

The corresponding discrete state-space equations are:

$$\begin{aligned} \mathbf{x}(k+1) &= \mathbf{A}\mathbf{x}(k) + \mathbf{B}\Delta\mathbf{u}(k+1) + \mathbf{F}\Delta\mathbf{v}(k+1), \\ \mathbf{y}(k) &= \mathbf{C}\mathbf{x}(k), \end{aligned}$$

where

$$\mathbf{A} = \begin{bmatrix} \Phi(T_s) & \Gamma_u & \Gamma_v \\ \mathbf{0}_{1,n_x} & 1 & 0 \\ \mathbf{0}_{1,n_x} & 0 & 1 \end{bmatrix}, \mathbf{B} = \begin{bmatrix} \Lambda_u \\ 1 \\ 0 \end{bmatrix}, \mathbf{F} = \begin{bmatrix} \Lambda_v \\ 0 \\ 1 \end{bmatrix},$$

$$\mathbf{C} = \begin{bmatrix} \mathbf{C}_c & 0 & 0 \\ \mathbf{0}_{n_y,1} & 1 & 0 \end{bmatrix}.$$

A.2 | System prediction

Denoting N as a length of the prediction horizon $T_h = NT_s$, the predicted output of the system is:

$$\underline{\mathbf{y}}(k) = \begin{bmatrix} \mathbf{y}(k+1|k) \\ \mathbf{y}(k+2|k) \\ \vdots \\ \mathbf{y}(k+N|k) \end{bmatrix},$$

that can be written in terms of the current state and future input increments:

$$\underline{\mathbf{y}}(k) = \mathcal{P}\mathbf{x}(k) + \mathcal{T}_u \Delta\mathbf{u}(k) + \mathcal{T}_v \Delta\mathbf{v}(k), \quad (\text{A.2})$$

where

$$\mathcal{P} = \begin{bmatrix} \mathbf{C}\mathbf{A} \\ \vdots \\ \mathbf{C}\mathbf{A}^N \end{bmatrix},$$

$$\mathcal{T}_u = \begin{bmatrix} \mathbf{C}\mathbf{B} & \mathbf{0} & \cdots & \mathbf{0} \\ \mathbf{C}\mathbf{A}\mathbf{B} & \mathbf{C}\mathbf{B} & \cdots & \mathbf{0} \\ \vdots & \vdots & \ddots & \vdots \\ \mathbf{C}\mathbf{A}^{N-1}\mathbf{B} & \mathbf{C}\mathbf{A}^{N-2}\mathbf{B} & \cdots & \mathbf{C}\mathbf{B} \end{bmatrix},$$

$$\mathcal{T}_v = \begin{bmatrix} \mathbf{C}\mathbf{F} & \mathbf{0} & \cdots & \mathbf{0} \\ \mathbf{C}\mathbf{A}\mathbf{F} & \mathbf{C}\mathbf{F} & \cdots & \mathbf{0} \\ \vdots & \vdots & \ddots & \vdots \\ \mathbf{C}\mathbf{A}^{N-1}\mathbf{B} & \mathbf{C}\mathbf{A}^{N-2}\mathbf{F} & \cdots & \mathbf{C}\mathbf{F} \end{bmatrix}.$$

A.3 | Formulation of the objective function

To maximise the electrical power, the objective function takes the form:

$$\begin{aligned} E_{t,t+T_h}^{\text{elec}} &= -\frac{3}{2} \int_t^{t+T_h} i_{\text{sq}}(\tau) V_{\text{sq}}(\tau) d\tau, \\ &= -\frac{3}{2} \int_t^{t+T_h} i_{\text{sq}}(\tau) u(\tau) d\tau. \end{aligned} \quad (\text{A.3})$$

This objective function can be discretised and written as [32]:

$$J(k) = \frac{1}{2} \underline{\mathbf{y}}^T(k) \mathbf{Q} \underline{\mathbf{y}}(k), \quad (\text{A.4})$$

where \mathbf{Q} is a block diagonal matrix defined as:

$$\mathbf{Q} = \begin{bmatrix} \mathbf{M} & & & \\ & \ddots & & \\ & & \mathbf{M} & \\ & & & \frac{1}{2}\mathbf{M} \end{bmatrix}, \quad \mathbf{M} = \begin{bmatrix} 0 & 0 & 0 \\ 0 & 0 & 1 \\ 0 & 1 & 0 \end{bmatrix}.$$

Using Equation (A2), the objective function can be formulated as a quadratic programming problem with respect to the optimised variable $\Delta\mathbf{u}(k)$:

$$J_1 = \frac{1}{2} \Delta\mathbf{u}^T \mathcal{T}_u^T \mathbf{Q} \mathcal{T}_u \Delta\mathbf{u} + \Delta\mathbf{u}^T \mathcal{T}_u^T \mathbf{Q} (\mathcal{P}\mathbf{x} + \mathcal{T}_v \Delta\mathbf{v}). \quad (\text{A.5})$$

As shown in [33], J_1 is not always convex, and can be convexified by adding diagonal terms to the Hessian matrix ($\mathcal{T}_u^T \mathbf{Q} \mathcal{T}_u$) leading to:

$$J_2 = J_1 + \lambda_{\Delta u} \Delta\mathbf{u}^T \Delta\mathbf{u}, \quad (\text{A.6})$$

where the penalty term $\lambda_{\Delta u}$ is usually set to the minimum eigenvalue of the Hessian matrix $\lambda_{\Delta u}^{\min}$.

Re-writing Equation (A6) in a standard form, the resultant objective function that is optimised at every time step k is:

$$J(k) = \frac{1}{2} \Delta\mathbf{u}^T \mathbf{H} \Delta\mathbf{u} + \mathbf{f}^T \Delta\mathbf{u}, \quad (\text{A.7})$$

where

$$\begin{aligned} \mathbf{H} &= \mathcal{T}_u^T \mathbf{Q} \mathcal{T}_u + 2\lambda_{\Delta u} \mathbf{I}, \\ \mathbf{f} &= \mathcal{T}_u^T \mathbf{Q} (\mathcal{P}\mathbf{x}(k) + \mathcal{T}_v \Delta\mathbf{v}(k)). \end{aligned} \quad (\text{A.8})$$

Only the first component of the optimised variable $\underline{\Delta \mathbf{u}}(k)$ is used at each time step to control the WEC.

A.4 | Constraints

The PMSM has limitations on the maximum DC-bus current of 481 A, and this constraint can be included in the formulation of the optimisation problem using the linear inequalities [29]:

$$\begin{bmatrix} \mathbf{M}_j \\ -\mathbf{M}_j \end{bmatrix} \mathcal{J}_j \underline{\Delta \mathbf{u}} = \begin{bmatrix} -\mathbf{M}_j \\ \mathbf{M}_j \end{bmatrix} (\mathcal{P} \mathbf{x} + \mathcal{J}_j \underline{\Delta \mathbf{v}}) + \mathbf{I}_{\max} \quad (\text{A.9})$$

where

$$\mathbf{M}_j = \begin{bmatrix} \mathbf{C}_j & & & \\ & \mathbf{C}_j & & \\ & & \dots & \\ & & & \mathbf{C}_j \end{bmatrix}, \quad (\text{A.10})$$

$$\mathbf{C}_j = [0 \quad 1 \quad 0].$$

A.5 | Simulation set-up

The WEC wave-to-wire model (11) is implemented in MATLAB/Simulink and solved using `ode23` solver with a variable time-step. The discretisation step for the MPC is set to $T_s = 0.1$ s, the prediction horizon is set to $T_h = 6$ s, the penalty term is set 10 times higher than the minimum eigenvalue of the Hessian matrix $\lambda_{\Delta u} = 10 \times \lambda_{\Delta u}^{\min}$. The linear quadratic programming problem is solved using an in-built MATLAB function `quadprog`. The wave excitation force and its changes, $\underline{\Delta \mathbf{v}}(k)$, are assumed to be perfectly estimated over the length of the prediction horizon. Irregular waves are modelled using Bretschneider spectrum [30] characterised by the significant wave height H_s and peak wave period T_p . The simulation time for each sea state is set to $(300 \times T_p)$ s, and the transition period of $(15 \times T_p)$ s is disregarded when calculating average power production.